Semnan University

Journal of Heat and Mass Transfer Research

Journal homepage: http://jhmtr.journals.semnan.ac.ir

Casson Fluid Flow with Variable Viscosity and Thermal Conductivity along Exponentially Stretching Sheet Embedded in a Thermally Stratified Medium with Exponentially Heat Generation

Animasaun Isaac Lare*[1]

[1] Department of Mathematical Sciences, Federal University of Technology, Akure, Ondo State, Nigeria.

PAPER INFO

History:

Received 10 July 2014
Received in revised form 5 December 2014
Accepted 8 February 2015

Keywords:
Casson fluid;
Variable viscosity;
Variable thermal conductivity;
Space dependent heat source;
Thermal stratification

A B S T R A C T

The motion of temperature dependent viscosity and thermal conductivity of steady incompressible laminar free convective (MHD) non-Newtonian Casson fluid flow over an exponentially stretching surface embedded in a thermally stratified medium are investigated. It is assumed that natural convection is induced by buoyancy and exponentially decaying internal heat generation across the space. The dimensionless temperature is constructed such that the effect of stratification can be revealed. Similarity transformations were employed to convert the governing partial differential equations to a system of nonlinear ordinary differential equations. The numerical solutions were obtained using shooting method along with the Runge-Kutta Gill method. The behaviour of dimensionless velocity, temperature and temperature gradient within the boundary layer has been studied using different values of all the controlling parameters. The numerical result show that increase in the magnitude of temperature dependent fluid viscosity parameter leads to an increase in velocity, decrease in temperature, decrease in temperature gradient near the wall and increase in temperature gradient far from the wall. The velocity profile increases, temperature distribution increases and temperature gradient increases near the wall only by increasing the magnitude of temperature dependent thermal conductivity parameter.

1. Introduction

The theoretical study of two dimensional non-Newtonian incompressible fluid flows over a surface with stretching or shrinking properties has taken the significant attention in the past few years due to its wide applications in engineering fields as well as in the industry. Some applications include the production of toothpaste, shampoo, custard solution, blood treatment, glass fibre production and design of the plastic films. Crane [1] investigated boundary layer flow past a stretching sheet whose velocity is proportional to the distance from the sheet. In fluid dynamics, fluids are divided into two broad groups which are Newtonian and non-Newtonian. Non-Newtonian transport phenomena arise in many fields of mechanical and chemical engineering and also in food processing. Some materials e.g. muds, condensed milk, glues, printing ink, emulsions, paints, sugar solution, shampoos and tomato paste exhibit almost all the properties of non-Newtonian fluids. One of the properties of Newtonian fluid is that coefficient of viscosity does not change with the rate of deformation of the fluid. This property can be found in the motion of water, kerosene and air. In addition, non-Newtonian fluids do not exhibit the property of Newtonian fluids where shear stress is directly proportional to shear rate. There are three broad

*Corresponding author: A. Lare, Federal University of Technology, Akure, Ondo State, Nigeria. Email: anizakph2007@gmail.com

classifications of non-Newtonian fluids. These are time-dependent, time-independent and viscoelastic fluids. The time-independent non-Newtonian fluids are those fluids in which the shear rate at a given point is a function of the stress at that point only. Examples are Casson, Bingham, Dilatant and Pseudo-plastic fluids. The governing equations of non-Newtonian fluids are highly nonlinear and much more complicated than those of Newtonian fluids. The More research is needed to investigate such fluids for understanding the flow characteristics. See Mukhopadhyay [2]. This rheological model was introduced originally by Casson [3] in his study on a flow equation for pigment oil-suspensions of printing ink. Bird et al. [4] investigated the rheology and flow of plastic fluid model which exhibits shear thinning characteristics, yield stress and high shear viscosity. Venkatesan et al. [5] stated that the blood shows Newtonian fluid's characteristics when it flows through the larger diameter arteries at the high shear rates, but it exhibits a significant non-Newtonian behaviour when it flows through the small diameter arteries at low shear rates.

Internal energy generation can be explained as a scientific method of generating heat energy within a body by a chemical, electrical or nuclear process. The natural convection induced by the internal heat generation is a common phenomenon in nature. Examples include motion in the atmosphere where heat is generated by absorption of sunlight. see Tasaka et al. [6]. Crepeau and Clarksean [7] carried out a similarity solution for a fluid with an exponentially decaying heat generation term and a constant temperature vertical plate under the assumption that the fluid has an internal volumetric heat generation. An exponential form is used to account for the internal energy generation term. It was reported that the effect of internal heat generation is important in several applications i.e. reactor safety analyses, fire and combustion studies. In many situations, there may be appreciable temperature difference between the surface and the ambient fluid. This necessitates the consideration of temperature dependent heat sources that may exert a strong effect on the heat transfer characteristics El-Aziz and Salem [8]. The study of the heat generation or absorption effects is important in view of several physical problems such as fluids under the exothermic or endothermic chemical reaction; although, the exact modeling of internal heat generation or absorption is completely difficult, some simple mathematical models can express its average behaviour for most physical situations see El-Aziz and Salem [9].

The thermal stratification can be defined as the scientific term that describes the layering of bodies of water based on their temperature. This concept divides water bodies about a surface/plate into three layers known as epilimnion, metalimnion and hypolimnion. The epilimnion is the highest and warmest layer; the metalimnion is the transition layer between the upper warm regions of the fluid and the cool layer near the bottom is the hypolimnion. Recently, many researchers have reported free convection flow over a surface/plate embedded in a thermally stratified medium due to its real life application.

Moorthy and Senthilvadivu [10] have studied the effect of variable viscosity on free convective flow of non-Newtonian power-law fluids along a vertical surface with the thermal stratification. It was reported that as the thermal stratification parameter increases the heat transfer rate also increases for $\theta_c > 0$ and $\theta_c < 0$. In the research, θ_c is the parameter characterizing the effect of temperature on viscosity. The flow, heat and nanoparticle mass transfer characteristics in the free convection from a vertical plate in a thermally linearly stratified nanofluid saturated non-Darcy porous medium under the convective boundary condition have been investigated by RamReddy et al. [11]. They assumed that the fluid flow is moderate, so the pressure drop is proportional to the linear combination of the fluid velocity and the square of the velocity. They reported that the fluid velocity and temperature increase as the thermal stratification parameter increases. A theoretical study on magnetohydrodynamic boundary layer flow with constant viscosity and the thermal conductivity towards an exponentially stretching sheet embedded in a thermally stratified medium subject to suction is investigated by Mukhopadhyay [12]. It was reported that increase in stratification parameter in the absence of suction and also in the presence of suction corresponds to decrease in temperature profiles and increase in temperature gradient. The convective boundary condition invoked upon temperature profile in [11] was removed; behaviour of the fluid flow was reconsidered and explained in [13]. The resulting system of equations was solved numerically by using an implicit finite difference method. It was reported that the positive values of the thermal stratification parameter have the tendency to increase the boundary layer thickness, due to the enhancement in the temperature difference between the plate and the free stream in the presence of the nanofluids [13].

In most of the published articles, Casson fluid flow along the heated surface has been treated with constant viscosity and thermal conductivity. The heat transfer is energy in transit due to the temperature difference; whenever there is a temperature difference in a medium or between two medium of difference temperature, the heat transfer must occur significantly. The temperature difference is the driving force for heat transfer. Hence, viscosity and thermal conductivity cannot be assumed as a constant. This fact shows the occurrence of a phase of the variable viscosity. Due to the nature and behaviour of Casson fluid flow, it may not flow very well along a vertical surface. The motivation to this study is to research more on the areas that have been neglected in other works of many researchers. This will provide results on the effects of variable viscosity and thermal conductivity, stratification parameter and exponentially decaying heat generation on velocity, temperature and temperature gradient of Casson flow along exponentially stretching vertical surface embedded in a thermally stratified medium.

The aim of this theoretical study is to unravel the effect of the emerging controlling parameters on velocity, temperature and temperature gradient of Casson fluid with variable viscosity and thermal conductivity in the boundary layer over a vertical surface embedded in a stratified medium with suction and exponentially decaying space dependent internal heat generation. The governing partial differential equations are modified and converted to nonlinear ordinary differential equations by using the suitable similarity transformations. The transformed self-seminar ODE's are solved by using the shooting method and quadratic interpolation. The effects of the embedded flow controlling parameters on the fluid velocity, temperature, temperature gradient and heat transfer rate have been demonstrated graphically and discussed. A comparative study is also presented.

2. Mathematical Formulation

A steady incompressible two-dimensional laminar free convective electrically conducting viscous fluid flow along a vertical exponentially stretching sheet embedded in a thermally stratified medium in the presence of suction is considered for a theoretical study. The vertical surface is elastic. The motion of an incompressible non-Newtonian fluid is induced by the stretching property of the vertical surface, buoyancy effect generated by gradients in the temperature field and space dependent internal heat generation. This occurs in view of the elastic properties of the surface parallel to the x −axis through equal and opposite forces when the origin is fixed at $x = y = 0$. A variable magnetic field $B(x) = B_o exp(x/2L)$ of constant intensity B_o is applied in a direction transverse to the plate and the electrical conductivity of the fluid is assumed to be small so that the induced magnetic field can be neglected in comparison to applied magnetic field. The surface temperature $T_W(x)$ is embedded in a thermally stratified medium of variable ambient temperature $T_\infty(x)$ where $T_W(x) > T_\infty(x)$. The following wall conditions and the free stream temperature embedded in a thermally stratified medium are stated in Mukhopadhyay [12].

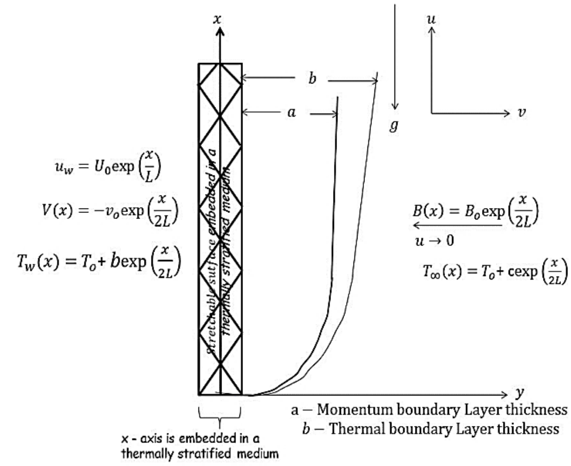

Figure 1. Physical model and coordinate system

Since the fluid pressure is constant throughout the boundary layer, it is assumed that the induced magnetic field is small in comparison to the applied magnetic field; hence it is neglected. Under the above assumptions and invoking the Boussinesq approximation, the boundary layer equations governing the flow and heat transfer of a viscous incompressible fluid can be written as

$$\frac{\partial u}{\partial x}+\frac{\partial v}{\partial y}=0 \tag{1}$$

$$u\frac{\partial u}{\partial x}+v\frac{\partial u}{\partial y}=\vartheta\frac{\partial^2 u}{\partial y^2}-\frac{\sigma\left[B(x)\right]^2}{\rho}u+g\beta^+\left(T-T_o\right) \tag{2}$$

$$u\frac{\partial T}{\partial x}+v\frac{\partial T}{\partial y}=\frac{\kappa}{\rho C_P}\frac{\partial^2 T}{\partial y^2}-\frac{1}{\rho C_P}\frac{\partial q_r}{\partial y}+\frac{Q_0}{\rho C_P}\left(T_W-T_o\right)e^{-ny\sqrt{\frac{U_o}{2\vartheta L}}\exp\left(\frac{x}{2L}\right)} \tag{3}$$

where T is the fluid temperature , $\vartheta = \mu/\rho$ is the kinematic viscosity, μ is the fluid viscosity and ρ is the fluid density, $\alpha = \kappa/\rho C_P$ is the thermal diffusivity with κ being the fluid thermal conductivity and C_P is the heat capacity at constant pressure. The dimensionless space internal heat generation term in energy equation is formulated by using the concept introduced in Salem and El-Aziz [9] where Q_o is known as a coefficient of the dimensionless space-dependent internal heat generation. From the concept of viscosity $\left(\tau = \mu(\partial u/\partial y|_{y=0}\right)$, according to Mukhopadhyay [14] and Hayat et al. [15] it is assumed that the rheological equation of an isotropic and incompressible flow of a Casson fluid can be written as

$$\tau_{ij} = \left(\mu_b + \frac{P_y}{\sqrt{2\pi}} \right) 2e_{ij} \quad when\ \pi > \pi_c \tag{4}$$
$$\tau_{ij} = \left(\mu_b + \frac{P_y}{\sqrt{2\pi_c}} \right) 2e_{ij} \quad when\ \pi < \pi_c$$

According to [12], P_y is known as the fluid yield stress that mathematically expresses as

$$P_y = \frac{\mu_b \sqrt{2\pi}}{\beta} \tag{5}$$

μ_b is known as the plastic dynamic viscosity of the non-Newtonian fluid, π is the product of the deformation rate component with itself i.e. $\pi = e_{ij}e_{ij}$, where e_{ij} is the $(i,j)th$ component of the deformation rate and π_c is the critical value of π based on non-Newtonian model. In a case of Casson fluid (non-Newtonian) flow, where $\pi > \pi_c$, it's possible to say that

$$\mu = \mu_b + \frac{P_y}{\sqrt{2\pi}} \tag{6}$$

Substituting (5) into (6) then simplify

$$\mu = \mu_b \left(1 + \frac{1}{\beta} \right)$$

The kinematics viscosity of Casson fluid is now a function depending on plastic dynamic viscosity, density and Casson parameter (β)

$$\vartheta = \frac{\mu_b}{\rho} \left(1 + \frac{1}{\beta} \right) \tag{7}$$

The Rosseland approximation requires that the media is optically dense media and the radiation travels only a short distance before being scattered or absorbed. The another objective of this research is to study the radiation of heat within optically thick Casson fluid before the heat is scattered, radiative heat transfer is taken into account, and the Rosseland equation is used to estimate the radiative thermal conductivity in Casson fluid. The Rosseland equation is a simplified model of Radiative Transfer Equation (RTE). When the material has a great extinction coefficient, it can be treated as optically thick. q_r is the radiative heat flux and is defined by using the Rosseland approximation Chamkha et al. [16] as

$$q_r = \frac{-4\sigma^*}{3k^*} \frac{\partial T^4}{\partial y} \tag{8}$$

where σ^* is the Stefan-Boltzmann constant and k^* is known as the absorption coefficient. By assuming that the temperature difference within the flow is such that T^4 may be expanded in a Taylor series and expanding T^4 about T_∞ and neglecting higher orders. Next is to consider Taylor Series Expansion of T^4 about T_∞, Considering the Taylor's series expansion of a function $f(x)$ about x_0

$$f(x) = f(x_0) + (x - x_0) f'(x_0)$$
$$+ \ldots \frac{(x - x_0)^n}{n!} f^n(x_0)$$

Likewise, expansion of T^4 about T_∞, by neglecting higher order

$$T^4 \approx T_\infty^4 + 4T_\infty^3 T - 4T_\infty^3 T_\infty \tag{9}$$

$$\frac{\partial q_r}{\partial y} = \frac{-16\sigma^* T_\infty^3}{3k^*} \frac{\partial^2 T}{\partial y^2} \tag{10}$$

In this study, it is assumed that the plastic dynamic viscosity μ_b and the thermal conductivity of Casson fluid κ vary as a linear function of temperature. This assumption is valid since it is known that the physical properties of the fluid may change significantly with temperature. For lubricating fluids, the heat generated by the internal friction and the corresponding rise in temperature affect on the fluid viscosity and so the fluid viscosity can no longer be assumed constant. In industry, the fluids can be subjected to extreme conditions such as high temperature, pressure, high shear rates and external heating (Ambient Temperature) and each of these factors can lead to high temperature being generated within the fluid. According to Anyakoha [17], Batchelor [18] and Vajravelu et at. [19]. The following relations are now introduced for u and v as $u = \frac{\partial \psi}{\partial y}$ and $v = -\frac{\partial \psi}{\partial x}$ respectively. Here ψ is the stream function. These automatically satisfy continuity equation (1). Modified governing equations of (2) and (3) are:

$$\frac{\partial \psi}{\partial y}\frac{\partial^2 \psi}{\partial x \partial y} - \frac{\partial \psi}{\partial x}\frac{\partial^2 \psi}{\partial y^2} = \frac{\mu_b(T)}{\rho}\left(1 + \frac{1}{\beta}\right)\frac{\partial^2 u}{\partial y^2} + g\beta^*(T - T_o) \tag{11}$$
$$+ \frac{1}{\rho}\left(1 + \frac{1}{\beta}\right)\frac{\partial^2 \psi}{\partial y^2}\frac{\partial \mu_b(T)}{\partial T}\frac{\partial T}{\partial y} - \frac{\sigma B(x)^2}{\rho}\frac{\partial \psi}{\partial y}$$

$$\frac{\partial \psi}{\partial y}\frac{\partial T}{\partial x} - \frac{\partial \psi}{\partial x}\frac{\partial T}{\partial y} = \frac{\kappa(T)}{\rho C_P}\frac{\partial^2 T}{\partial y^2} + \frac{1}{\rho C_P}\left(\frac{\partial T}{\partial y}\right)^2 \frac{\partial \kappa(T)}{\partial T} + \tag{12}$$
$$\frac{16\sigma^* T_\infty^3}{3\rho C_P k^*}\frac{\partial^2 T}{\partial y^2} + \frac{Q_0}{\rho C_P}(T_W - T_0)\, e^{-ny\sqrt{\frac{U_o}{2\vartheta L}}\exp\left(\frac{x}{2L}\right)}$$

In Physics, it is a well-known fact that, if an object is on an elastic surface at rest, when the surface is stretched; the object also tends to move towards the direction of the pull. The surface of the plate is assumed to be highly elastic and is stretched in the vertical x −direction with velocities

$$u = u_w(x) = U_0 \exp\left(\frac{x}{L}\right), v_w(x) = v_o \exp\left(\frac{x}{2L}\right),$$
$$T_w(x) = T_0 + b\exp\left(\frac{x}{2L}\right), T_\infty(x) = T_0 + c\exp\left(\frac{x}{2L}\right)$$

T_o is the reference temperature, $b > 0$ and $c \geq 0$ are constants. Equations (11) and (12) are subject to following boundary conditions

$$u = u_w(x), v = -v_w(x), T = T_w(x) \, at \, y = 0 \tag{13}$$

$$u \to 0 \; ; \; T \to T_\infty(x) \quad as \quad y \to \infty \tag{14}$$

In this study, U_0 is a constant and L is the reference length. It is very important to note that, the exponential velocity $U_0 \exp(x/L)$ is valid only when $x \ll L$. When $x \geq L$, it is obvious that the effect of the exponential property on wall velocity may skyrocket. Also, in the third term of Equation (13); it is obvious that $(T_w - T_0) = b\exp(x/2L)$, $(T_\infty - T_0) = c\exp(x/2L)$. By introducing the stream function $\psi(x, y)$ and similarity variables η as

$$\psi = \sqrt{2\vartheta L U_0} f(\eta) \exp\left(\frac{x}{2L}\right),$$
$$\eta = y\sqrt{\frac{U_0}{2\vartheta L}} \exp\left(\frac{x}{2L}\right) \tag{15}$$

Dimensionless temperature, thermal conductivity model in Salem and Fathy [20] temperature dependent viscosity model in Layek et al. [21] and respectively as

$$\theta(\eta) = \frac{T - T_\infty}{T_w - T_0}, \; \kappa(T) = \kappa^*\left[1 + \delta(T - T_\infty)\right],$$
$$\mu_b(T) = \mu_b^*\left[1 + \tau(T_w - T)\right] \tag{16}$$

By substituting all into Equations (11) to (14) we obtain the following locally similar ordinary differential equations:

$$\left(1 + \frac{1}{\beta}\right)\left[1 + \xi - \theta\xi - \xi S_t\right] f''' - \xi\left(1 + \frac{1}{\beta}\right)\theta' f''$$
$$-2f'f' + ff'' - H_a f' + G_{rm}\theta\xi = 0 \tag{17}$$

$$\left[1 + \frac{4}{3N} + \theta\varepsilon\right]\theta'' + \varepsilon\theta'\theta' - S_t P_r f'$$
$$-P_r\theta f' + P_r f\theta' + P_r q_1 e^{-n\eta} = 0 \tag{18}$$

Together with the boundary conditions

$$f'(\eta) = 1, f(\eta) = S, \theta(\eta) = 1 - S_t, \; at \; \eta = 0 \tag{19}$$

$$f'(\eta) \to 0, \; \theta(\eta) \to 0 \quad as \quad \eta \to \infty \tag{20}$$

Here all the primes denote the differentiation with respect to η, $\xi = \tau(T_w - T_0)$ is known as temperature dependent variable plastic dynamic viscosity parameter, $\beta = \frac{\mu_b\sqrt{2\pi}}{P_y}$ is the non-Newtonian Casson parameter, $G_{rm} = \frac{2g\beta^+ L}{\gamma {U_0}^2 \exp\left(\frac{2x}{L}\right)}$ is the local modified Grashof related parameter, $\varepsilon = \delta(T_w - T_o)$ is known as temperature dependent variable thermal conductivity parameter, $N = \frac{4\sigma^* T_\infty^3}{\kappa k^*}$ is known as thermal radiation parameter, $P_r = \frac{C_p\mu}{\kappa}$ is the Prandtl number, $q_1 = \frac{2LQ_0}{U_0\rho C_P \exp\left(\frac{x}{L}\right)}$ is the space dependent internal heat source parameter and $S_t = c/b$ is the stratification parameter. For practical applications, the major physical quantities of interest are the local skin friction coefficient and Nusselt number. The first physical quantity of interest is the wall skin friction coefficient C_f defined as

$$C_f = \frac{\tau_w}{\rho {U_0}^2 \exp(x/2L)}, \; \tau_w = \left(\mu_B + \frac{P_y}{\sqrt{2\pi}}\right)\frac{\partial u}{\partial y}\bigg|_{y=0}$$

τ_w is known as the shear stress or the skin friction along the stretching sheet

$$\sqrt{2}\exp\left(\frac{x}{2L}\right)\sqrt{R_{ex}}C_f = \left(1 + \frac{1}{\beta}\right)f''(0) \tag{21}$$

Another physical quantity of interest is the local Nusselt number Nu_x, which is defined as

$$Nu_x = \frac{Lq_w}{\kappa(T_w - T_\infty)} \; ; \; q_w = -\kappa\frac{\partial T}{\partial y}\bigg|_{y=0} \tag{22}$$

q_w is known as heat flux from the sheet

$$\exp(x/2L)\frac{Nu_x}{\sqrt{R_{ex}}} = -\theta'(0) \tag{23}$$

Here local Reynold number $R_{ex} = \frac{U_0 L}{\vartheta}$.

3. The Numerical Technique

The set of strong non-linear coupled differential equations (17) and (18) together with the boundary conditions (19) and (20) are solved numerically by using Runge Kutta Gill method along with shooting techniques by using the prescribed parameters. The quadratic interpolation is based on local approximation of the nonlinear functions in RHS of (25)-(29) by a quadratic function and the root of the quadratic function is taken as an improved approximation to the root of nonlinear functions. The procedure is applied repetitively to converge. There are two types of error involved in Runge Kutta as an approximation method of ordinary differential equations. They are round off error and truncation error. Runge Kutta Gill method is selected because it reduces (minimize) round off error and this method of the integration systems of first order does not require preceding function values to be known see Gill [22]. According to Finlayson [23], Order analysis, Consistency analysis and Stability analysis shows that Runge Kutta Gill is also of fourth order, stable and consistent. The constants are selected to reduce the amount of storage required in the solution of a large number of simultaneous first order differential equation, in addition; the Runge Kutta Gill variant method is probably used more often in machine integration due to the storage saving. The BVP cannot be solved on an infinite interval, and it would be impractical to solve it on a very large finite interval. In this study, the author imposed the infinite boundary condition at a finite point of $\eta = 8$. By following Na [24], superposition method is adopted to reduce the governing dimensionless equations, (17) and (18) together with boundary conditions (19) and (20) to system of first order nonlinear autonomous ordinary differential equations. Let

$$f = F^1, f' = F^2, f'' = F^3, \theta = \theta^1 \text{ and } \theta' = \theta^2 \tag{24}$$

Now becomes

$$\frac{dF^1}{d\eta} = F^2 \qquad F^1(0) = S \tag{25}$$

$$\frac{dF^2}{d\eta} = F^3 \qquad F^2(0) = 1 \tag{26}$$

$$\frac{dF^3}{d\eta} = \frac{\xi\left(1+\frac{1}{\beta}\right)\theta^2 F^3 + 2F^2F^2 - F^1F^3 + H_aF^2 - G_{rm}\theta^1\xi}{\left(1+\frac{1}{\beta}\right)\left[1+\xi-\theta^1\xi-\xi S_t\right]} \tag{27}$$

$$F^3(0) = Guess1$$

$$\frac{d\theta^1}{d\eta} = \theta^2 \qquad \theta^1(0) = 1 - S_t \tag{28}$$

$$\frac{d\theta^2}{d\eta} = \frac{-\varepsilon\theta^2\theta^2 + S_tP_rF^2 + P_r\theta F^2 - P_rF^1\theta^2 - P_rq_1e^{-n\eta}}{1+\frac{4}{3N}+\theta^1\varepsilon} \tag{29}$$

$$\theta^2(0) = Guess2$$

According to the shooting method, equation (20) is used to obtain Guess 1 and Guess 2. To integrate the corresponding IVP (25) to (29), Guess 1 and Guess 2 are required but no such values exist after the non-dimensionalization of the boundary conditions. The suitable guess values are chosen and then the integration is carried out. The calculated values for $f'(\eta = 8)$ and $\theta(\eta = 8)$ are compared with that of boundary condition (20). The interpolation is employed and the better estimation for Guess 1 and Guess 2 are obtained, IVP are solved by using the Runge Kutta Gill method with $\mathrm{h} = 0.1$. To improve the solutions, quadratic interpolation method which is superior (i. e. faster convergence rate) is adopted more than linear interpolation namely secant method Hoffman [25]. In very sensitive problems like this, the quadratic interpolation may misbehave and require bracketing techniques Hoffman [25]. Hence, the guess values were chosen wisely. The above procedure is repeated until results up to the desired degree of accuracy 0.000001 is obtained. From the numerical computation, Guess 1 is proportional to the skin-friction coefficient and Guess 2 is proportional to Nusselt Number, which are $\left(1+\frac{1}{\beta}\right)f''(0)$ and $-\theta'(0)$. They are also sorted out and their values are presented in a tabular form.

4. Results and Discussion

In order to analyse the numerical results, the computation have been carried out by using the method described in the previous section for various values of the temperature dependent plastic dynamic variable viscosity parameter (ξ), non-Newtonian Casson parameter (β), local modified Grashof related parameter (G_{rm}), the temperature dependent variable thermal conductivity parameter (ε), thermal radiation parameter (N) Prandtl number (P_r), space dependent internal heat source parameter $(q1)$, intensity of internal heat generation parameter on space (n) and stratification parameter (S_t). In order to show the results, the numerical values were plotted in figures 2 to 22. For the accuracy verification of the applied numerical scheme, has been made a comparison of the present results corresponding to the values of heat transfer coefficient $-\theta'(0)$ for the thermal radiation parameter values (N) and Prandtl number (P_r) with the available published results of Bidin and Nazar [26], Nadeem et al. [27] and Pramanik [28] when $\xi = G_{rm} = H_a = \varepsilon = q1 = S_t = S = 0$ and $\beta = \infty$. It is very important to note that in all of the above mentioned study $N = \kappa k^*/4\sigma T_\infty^3$ and in this present study $N = 4\sigma T_\infty^3/\kappa k^*$. Table 1 shows the good agreement between the present study result and the results reported by [27 - 29]. The numerical values of $\left(1+\frac{1}{\beta}\right)f''(0)$ and $-\theta'(0)$ for five different values of the temperature dependent variable plastic dynamic viscosity parameter (ξ), temperature dependent thermal conductivity of the Casson fluid parameter (ε), Stratification parameter (S_t), the non-Newtonian Casson fluid parameter (β), The space dependent internal heat source parameter (q_1) and the magnetic field parameter (H_a) are shown in Table 2 to 7.

4.1 The Velocity Profiles

Figure 2 illustrates the velocity profiles for the different values of temperature dependent plastic dynamic viscosity parameter (ξ) when magnetic field is present (i.e. $H_a = 0.2$), the wall temperature is 0.2 (since $S_t = 0.8$) and in the presence of suction $(S = 0.3)$.

Table 1a: Various values of $-\theta'(0)$ for several values of Prandtl number P_r and thermal radiation N

P_r	Bidin and Nazar [26] with $E = 0$ and $N = 0.5$	Bidin and Nazar [26] with $E = 0$ and $N = 1$	Nadeem et al. [27] for PES case with E = λ1 = 0 B = ω = 0 and N = 0.5	Nadeem et al. [27] for PES case with E = λ1 = 0 B = ω =0and N = 1
1	0.6765	0.5315	0.680	0.534
2	1.0735	0.8627	1.073	0.863
3	1.3807	1.1214	1.381	1.121

Table 1b: Various values of $-\theta'(0)$ for several values of Prandtl number P_r and thermal radiation N

P_r	Pramanik [28] with $S = 0$ and N = 0.5	Pramanik [28] with $S = 0$ and N = 1	Present Study when $N = 0.5$	Present Study when $N = 1$
1	0.6765	0.5315	0.6796065524	0.54043265
2	1.0734	0.8626	1.0735232305	0.86330896
3	1.3807	1.1213	1.3807094061	1.121406344

Table 2: The numerical values of skin friction $\left(1+\frac{1}{\beta}\right)f''(0)$ and Nusselt number $-\theta'(0)$ for different values of ξ when $\beta = 0.2$, $G_r = 1$, $H_a = 0.2$, $\varepsilon = 0.3$, $S_t = 0.8$, $N = 0.1$, $P_r = 0.72$, $q_1 = 4$, $n = 0.5$ and $S = 0.3$

	$\left(1+\frac{1}{\beta}\right)f''(0)$	$-\theta'(0)$
$\xi = 0$	-0.58033315366	-0.19297988839
$\xi = 1$	-0.47865821488	-0.17595041513
$\xi = 2$	-0.39814367596	-0.16415899336
$\xi = 3$	-0.32987792423	-0.15498693759
$\xi = 4$	-0.26998929605	-0.14742128026

Table 3: The numerical values of skin friction $\left(1+\frac{1}{\beta}\right)f''(0)$ and Nusselt number $-\theta'(0)$ for different values of ε when $\beta = 0.2$, $G_r = 1$, $H_a = 0.2$, $\xi = 7$, $S_t = 0.1$, $N = 0.1$, $P_r = 0.72$, $q_1 = 2$, $n = 0.5$ and $S = 0.3$

	$\left(1+\frac{1}{\beta}\right)f''(0)$	$-\theta'(0)$
$\varepsilon = 0$	0.38029408146	0.13950363697
$\varepsilon = 2$	0.39608728939	0.13306308069
$\varepsilon = 4$	0.41022951875	0.12769681385
$\varepsilon = 6$	0.42297898314	0.12313492843
$\varepsilon = 8$	0.43453770806	0.11919401705

Table 4: The numerical values of skin friction $\left(1+\frac{1}{\beta}\right)f''(0)$ and Nusselt number $-\theta'(0)$ for different values of S_t when $\beta = 0.2$, $G_r = 1$, $H_a = 0.2$, $\xi = 5$, $\varepsilon = 0.3$, $N = 0.1$, $P_r = 0.72$, $q_1 = 4$, $n = 0.5$ and $S = 0.3$

	$\left(1+\frac{1}{\beta}\right)f''(0)$	$-\theta'(0)$
$S_t = 0.1$	0.2423454704	0.0039531174
$S_t = 0.3$	0.1071762460	-0.0351964237
$S_t = 0.5$	-0.0254888652	-0.0758496008
$S_t = 0.7$	-0.1541973060	-0.1185592298
$S_t = 0.9$	-0.2762632257	-0.1642878981

Table 5a: The numerical values of skin friction $\left(1+\frac{1}{\beta}\right)f''(0)$ and Nusselt number $-\theta'(0)$ for different values of β when $G_r = 1$, $H_a = 0.2$, $\epsilon = 0.3$, $N = 0.1$, $P_r = 0.72$, $q_1 = 4$, $n = 0.5$, $S = 0.3$, with stratification i. e. $S_t = 0.8$ and Constant viscosity i.e. $\xi = 0$

	$\left(1+\frac{1}{\beta}\right)f''(0)$	$-\theta'(0)$
$\beta = 0.2$	-0.5803331536	-0.1929798883
$\beta = 0.4$	-0.7683601849	-0.2087962015
$\beta = 0.6$	-0.8871396114	-0.2165450766
$\beta = 0.8$	-0.9711797061	-0.2212170852
$\beta = \infty$	-1.5083186193	-0.2408359712

Table 5b: The numerical values of skin friction $\left(1+\frac{1}{\beta}\right)f''(0)$ and Nusselt number $-\theta'(0)$ for different values

of β when $G_r = 1, H_a = 0.2, \epsilon = 0.3, N = 0.1, P_r = 0.72, q_1 = 4, n = 0.5, S = 0.3$, without stratification i. e. $S_t = 0$ and variable viscosity i.e. $\xi = 4$		
	$\left(1+\frac{1}{\beta}\right)f''(0)$	$-\theta'(0)$
$\beta = 0.2$	0.1614976127	0.0131299811
$\beta = 0.4$	0.3099329276	0.0208077049
$\beta = 0.6$	0.3977222612	0.0239636390
$\beta = 0.8$	0.4578108659	0.0256996181
$\beta = \infty$	0.8166745975	0.0318467183

Table 6a: The numerical values of skin friction $\left(1+\frac{1}{\beta}\right)f''(0)$ and Nusselt number $-\theta'(0)$ for different values of q_1 when $\beta = 0.2, G_r = 1, H_a = 0.2, \xi = 5, \varepsilon = 0.3, N = 0.1, P_r = 0.72, St = 0.2, n = 0.5$ and $S = 0.3$

	$\left(1+\frac{1}{\beta}\right)f''(0)$	$-\theta'(0)$
$q_1 = -4$	−0.4021777440	0.4917324422
$q_1 = -3$	−0.3061302489	0.4259798427
$q_1 = -2$	−0.2175207354	0.3609687208
$q_1 = -1$	−0.1359439315	0.2966553138
$q_1 = 0$	−0.0610880340	0.2330037758
$q_1 = 1$	0.0072755257	0.1699856508
$q_1 = 2$	0.0692967214	0.1075787123
$q_1 = 3$	0.1250469780	0.0457671841
$q_1 = 4$	0.1745109835	−0.0154589350
$q_1 = 5$	0.2175685863	−0.0761031161

Table 7: The numerical values of skin friction $\left(1+\frac{1}{\beta}\right)f''(0)$ and Nusselt number $-\theta'(0)$ for different values of H_a when $\beta = 0.2, G_r = 1, \xi = 5, \varepsilon = 0.3, N = 0.1, P_r = 0.72, q_1 = 4, n = 0.5, S = 0.3$ and without stratification i. e. $S_t = 0$

	$\left(1+\frac{1}{\beta}\right)f''(0)$	$-\theta'(0)$
$H_a = 1$	0.1683000586	0.0118356128
$H_a = 2$	0.0106286718	−0.0007416954
$H_a = 3$	−0.1288065456	−0.0118566444
$H_a = 4$	−0.2535527859	−0.0216948097
$H_a = 5$	−0.3663604977	−0.0304266067

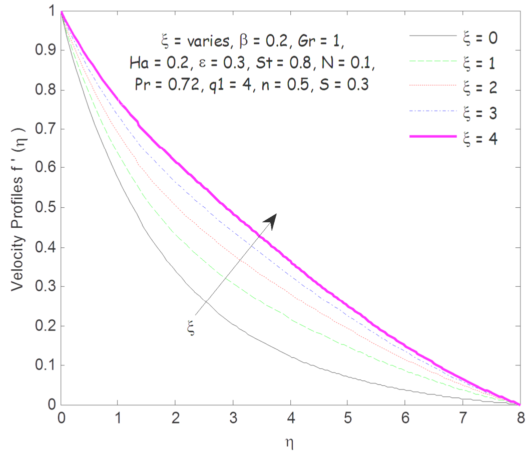

Figure 2. Effects of the variable plastic dynamic viscosity parameter (ξ) over the Velocity

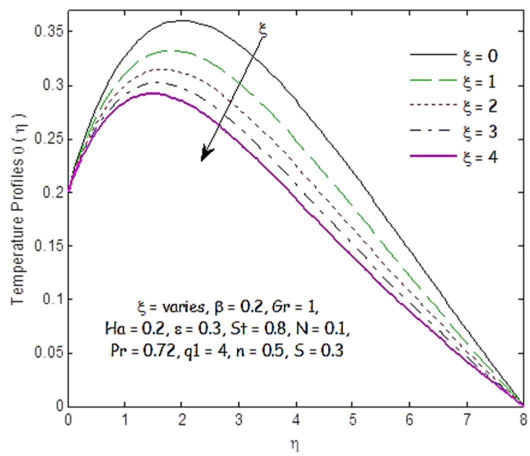

Figure 3. Effects of the variable plastic dynamic viscosity parameter (ξ) over the Temperature profiles

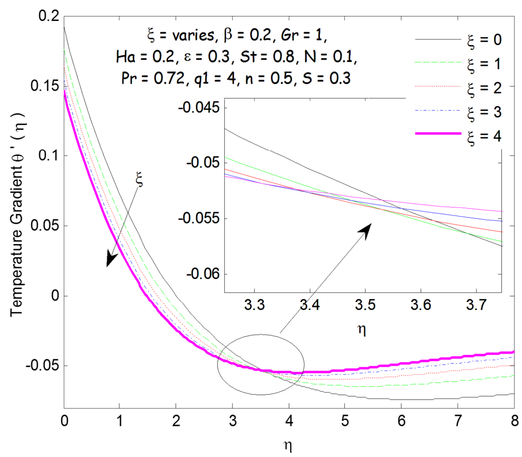

Figure 4. Effects of the variable plastic dynamic viscosity parameter (ξ) over the Temperature gradients

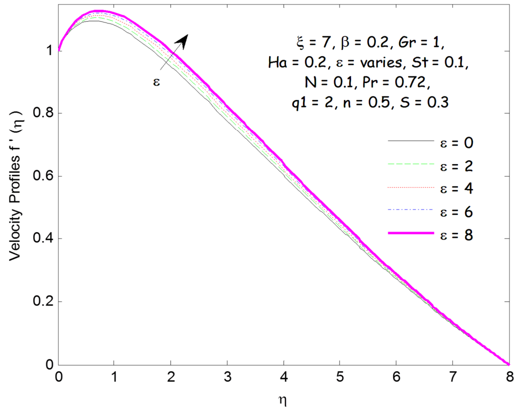

Figure 5. Effects of the variable thermal conductivity parameter (ε) over the Velocity profiles

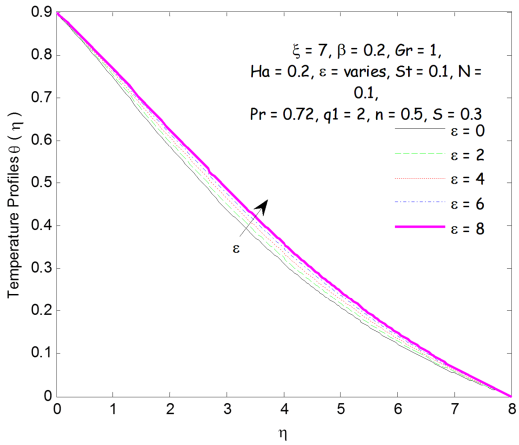

Figure 6. Effects of the variable thermal conductivity parameter (ε)over the Temperature profiles

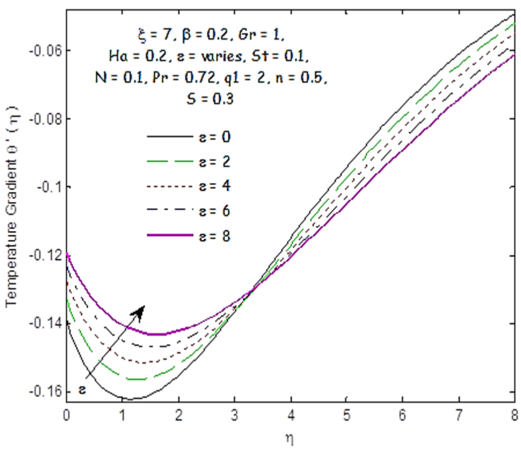

Figure 7. Effects of the variable thermal conductivity parameter (ε) over the Temperature gradients

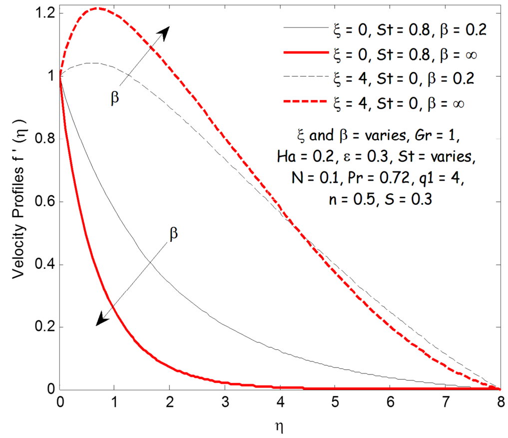

Figure 8. Effects of non-Newtonian Casson parameter (β) over Velocity profiles

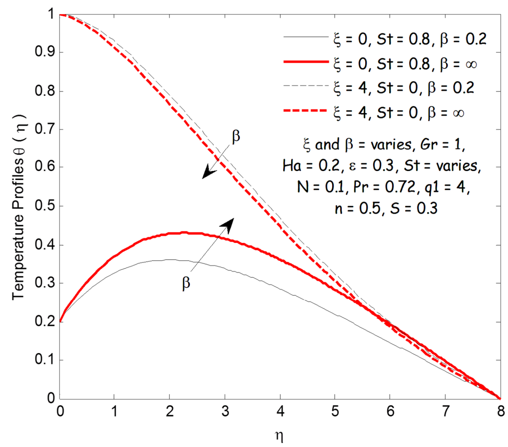

Figure 9. Effects of the non-Newtonian Casson parameter (β) over Temperature profiles

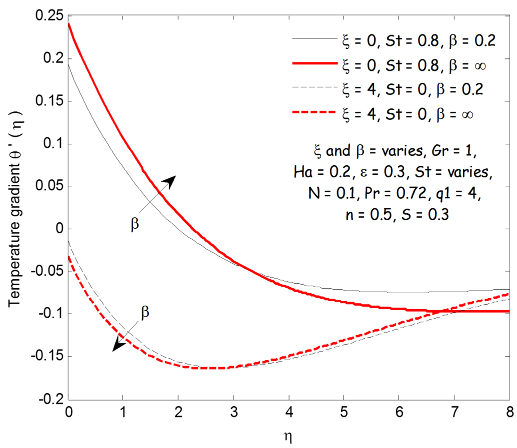

Figure 10. Effects of the the non-Newtonian Casson parameter (β) over Temperature gradients

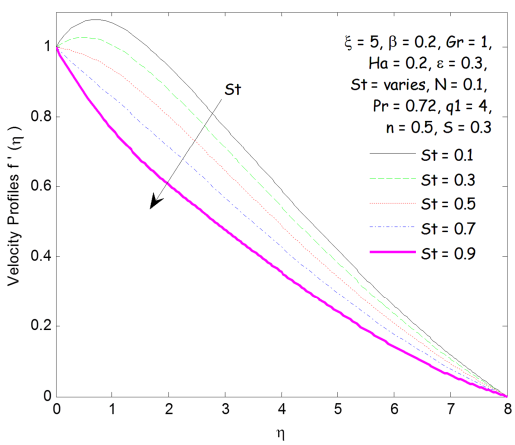

Figure 11. Effects of the Stratification parameter (S_t) over Velocity profiles

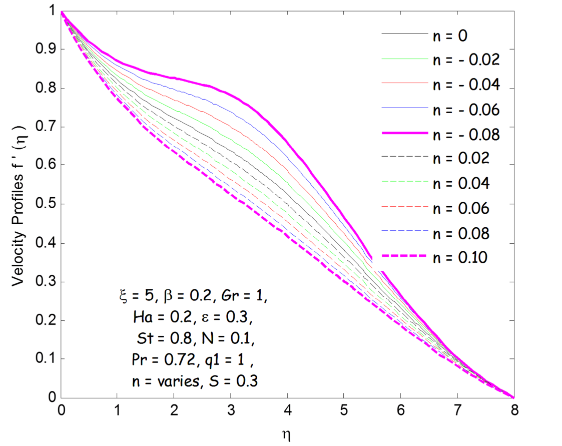

Figure 14. Effects of the intensity of the internal heat generation parameter on space (n) over Velocity profiles

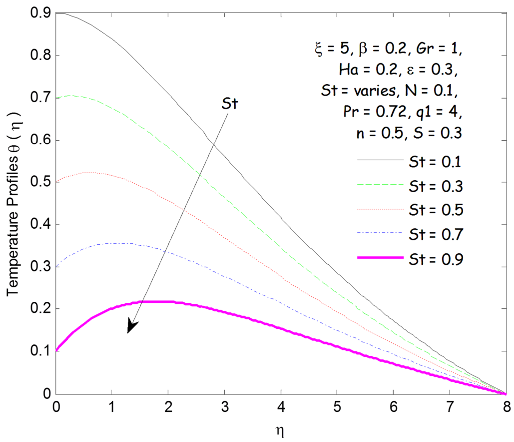

Figure 12. Effects of the Stratification parameter (S_t) over Temperature profiles

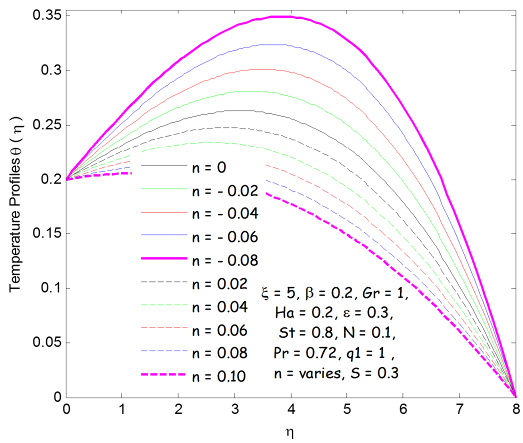

Figure 15. Effects of the intensity of internal heat generation parameter on space (n) over Temperature profiles

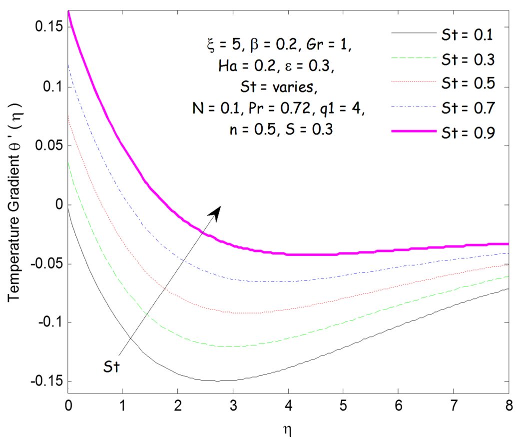

Figure 13. Effects of the Stratification parameter (S_t) over Temperature gradients

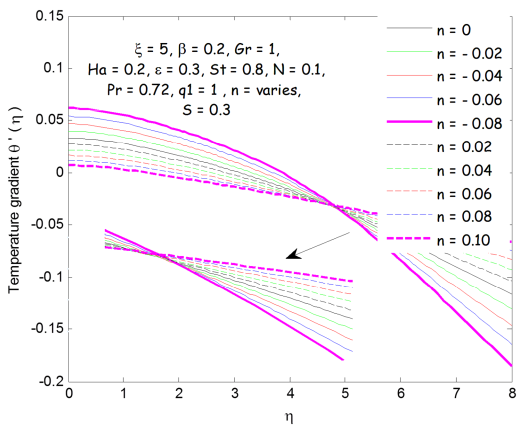

Figure 16. Effects of the intensity of the internal heat generation parameter on space (n) over Temperature gradients

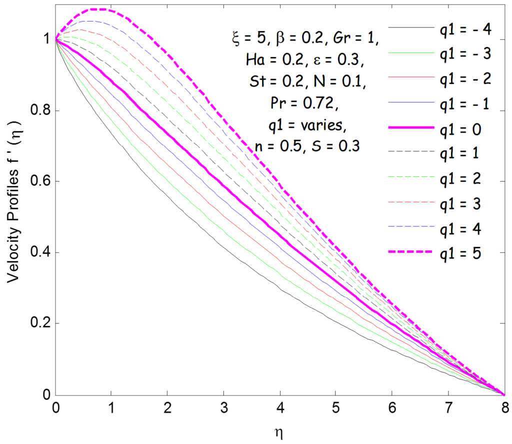

Figure 17. Effects of the internal heat generation parameter on space (q_1) over Velocity profiles

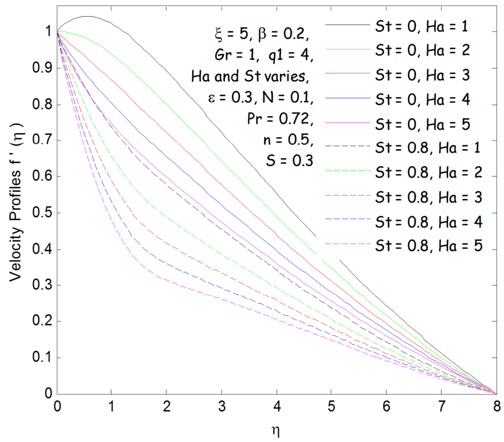

Figure 20. Effects of the Magnetic field parameter (H_a) with and without stratification over Velocity profile

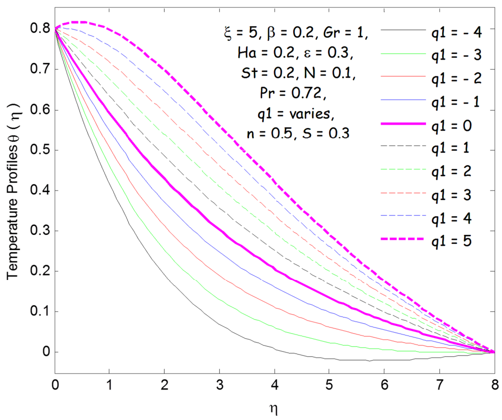

Figure 18. Effects of the internal heat generation parameter on space (q_1) over Temperature profiles

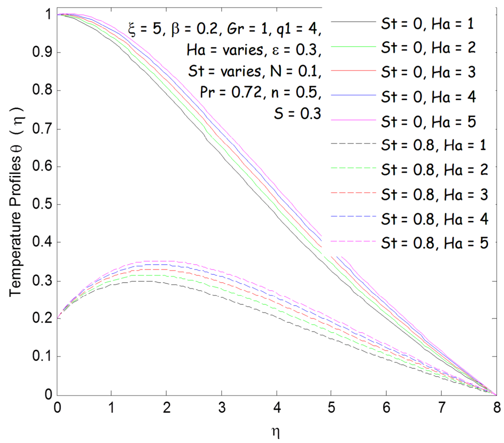

Figure 21. Effects of the Magnetic field parameter (H_a) with and without stratification over Temperature profiles

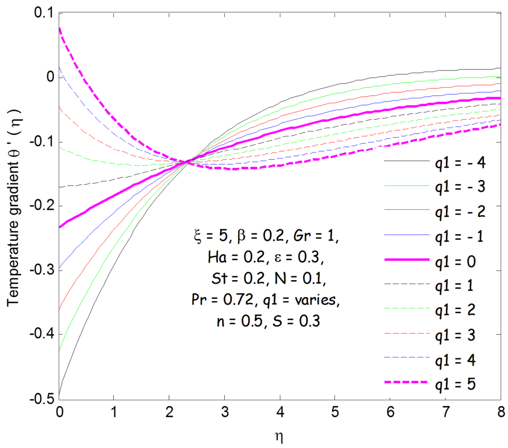

Figure 19. Effects of the internal heat generation parameter on space (q_1) over Temperature gradients

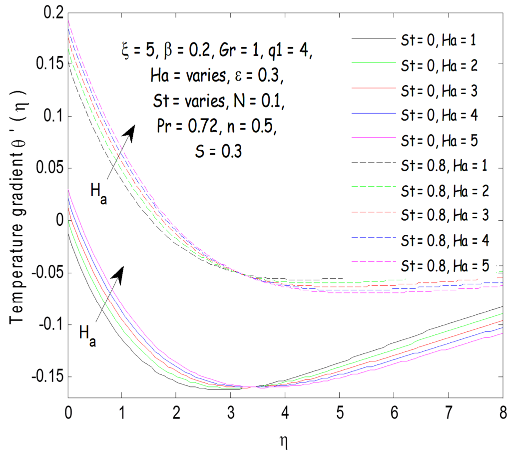

Figure 22. Effects of the Magnetic field parameter (H_a) with and without stratification over Temperature gradient

It is observed that when Casson fluid is considered as the fluid with constant plastic dynamic viscosity, the velocity is found to be very small in magnitude throughout the boundary layer compare to when considered as variable plastic dynamic viscosity. This figure demonstrates the effect of increasing ξ i.e. to increase the resulting temperature difference $(T_w - T_o)$ which makes the intermolecular forces (bond) between the Casson fluid to become weaker and drastically decreases the strength of plastic dynamic viscosity. This effect eventually increases the transport phenomena across the momentum boundary layer. From Figure 5 it is observed that as the temperature dependent variable thermal conductivity parameter (ε) increases, the velocity profiles increases. Effect of parameter (ε) is more negligible few distances away from the wall. This effect is due to increment in temperature difference between temperature at the wall and reference temperature. Maximum velocity is found very close to the surface that is embedded in a thermal stratification (i.e. $S_t = 0.1$). When the problem is investigated using high value of stratification parameter ($S_t = 0.8$), together with the same values of the remain parameters (i.e. $\xi = 7$, $\beta = 0.2$, $G_r = 1$, $H_a = 0.2$, $0 \leq \varepsilon \leq 8$, $N = 0.1$, $P_r = 0.72$, $q_1 = 2$, $n = 0.5$ and $S = 0.3$); it is observed that parameter (ε) has no significant effect on velocity profile of Casson fluid flow.

In order to investigate the dynamic of Casson fluid flow over a surface embedded in a thermally stratified medium, two different cases were considered at a fixed value of $G_{rm} = 1$, $H_a = 0.2$, $\varepsilon = 0.3$, $N = 0.1$, $P_r = 0.72$, $q_1 = 4$, $n = 0.5$ and $S = 0.3$. Figure 8 depicts both cases. In the first case, Casson fluid is considered as fluid with constant plastic dynamic viscosity (i.e. $\xi = 0$) when stratification parameter (i.e. $S_t = 0.8$). The velocity decreases with an increase in the value of β throughout the fluid domain ($0 \leq \eta \leq 8$). Increase in St means increase in free stream temperature (c) or decrease in surface temperature (b). It is obvious that both cases could not produce sufficient temperature to break down the molecules which makes up plastic dynamic viscosity; hence the velocity decreases since the viscosity of non-Newtonian Casson fluid is naturally high. In the second case, Casson fluid is treated as fluid with variable plastic dynamic viscosity (i.e. $\xi = 4$) without stratification (i.e. $St = 0$), the velocity increases very close to the wall ($0 \leq \eta \leq 4.357$) and after this interval velocity decreases as β increases from non-Newtonian fluid to Newtonian fluid (i.e. $\beta \to \infty$). The result is obvious for this case, $St = 0$ means the temperature of the exponentially stretching surface $\theta(\eta = 0) = 1$ and more heat is injected since $\xi = \tau(T_w - T_0) = 4$; hence the intermolecular forces within plastic dynamic viscosity is broken.

Next, the effects of thermal stratification parameter (S_t) on velocity profiles of non-Newtonian Casson fluid $(\beta = 0.2)$ when heat is injected greatly by setting ($\xi = 5$), in the presence of magnetic field $(Ha = 0.2)$ and uniform suction $(S = 0.3)$. It is found that velocity decreases. This result can be traced to the fact that, as (St) increases, the surface temperature within thermally stratified medium ranges from epilimnion to hypolimnion. Since the wall temperature decreases, coldness is introduced and this makes the molecules and intermolecular forces of Casson fluid to become stronger. This explains the decrement in velocity with an increase in S_t.

Figure 14 exhibits the velocity profiles for different values of intensity of internal heat generation parameter (n). The velocity decreases as n ranges from -0.08 to 0. This parameter is further investigated within $0.02 \leq n \leq 0.10$; the velocity profiles decreases as n increases. Figure 17 exhibits the velocity profiles for different values of exponentially decaying internal heat generation parameter when $\xi = 5$ and $\beta = 0.2$. The velocity increases as $q1$ ranges from -4 to 0. This parameter is further investigated within $1 \leq q1 \leq 5$; the velocity profiles increases as $q1$ increases. Figure 20 represents the velocity profiles for the variation of magnetic field parameter Ha with thermal stratification $(i.e. S_t = 0.8)$ and without thermal stratification$(i.e. S_t = 0)$. In both cases, the velocity decreases. Application of a magnetic field to an electrically conducting Casson fluid produces a kind of drag-like force called Lorentz force. This force causes reduction in the fluid velocity within boundary layer. The effect of Lorentz force on velocity profiles is highly experienced when thermal stratification is set to hypolimnion (i.e.$S_t = 0.8$). It is also observed that maximum velocity exist when thermal stratification is adjusted to epilimnion (i.e.$S_t = 0$)

4.2 Temperature Profiles

In Figure 3, variations of temperature field $\theta(\eta)$ against η for several values of ξ by using $Pr = 0.72$, $q1 = 4$ and $n = 0.5$ are shown. This figure indicates the drastic effect of the internal heat generation intensity across the space. The parabolic profiles of the temperature distribution with the pick slightly far from the wall are found to be lower when $\xi = 4$. It is observed that the temperature decreases as $\eta \to 8$. The increase of temperature dependent plastic dynamic viscosity parameter leads to decrease of thermal boundary layer thickness, which results in decreasing of temperature profile $\theta(\eta)$. Decrease in temperature profiles across the thermal boundary layer means a decrease in the velocity of the Casson fluid. In fact, in this case, the fluid particles undergo two opposite forces which are: (i) one force increases the fluid velocity due to decrease in the fluid viscosity with increase in the values of ξ, (ii) the second force decreases the fluid velocity due to decrease in temperature; since $\theta(\eta)$ decreases with increasing ξ. Very close to the vertical surface, as the temperature $\theta(\eta)$ is high, the first force dominates and far away from the surface, the temperature $\theta(\eta)$ is low; this implies that the second force dominates in that region.

From Figure 6 it is observed that as the temperature dependent variable thermal conductivity parameter ε increases, the temperature distribution increases significantly within the space. The effect of ε is negligible very close to the wall and also far from the wall when the value of the stratification ($S_t = 0.1$) and also far from the wall. When the problem is investigated again by using high value of stratification parameter ($S_t = 0.8$), together with the same values of the remain parameters i.e. $\xi = 7$, $\beta = 0.2$, $G_r = 1$, $H_a = 0.2$, $0 \leq \varepsilon \leq 8$, $N = 0.1$, $P_r = 0.72$, $q_1 = 2$, $n = 0.5$ and $S = 0.3$; it is observed that ε has no significant effect on temperature profile of Casson fluid flow. Figure 9 shows the effects of non-Newtonian Casson fluid parameter (β) on the temperature $\theta(\eta)$ for fixed values of ε, N, P_r, q_1, n and uniform suction. In order to investigate the dynamic of Casson fluid flow along with a vertical surface, two different cases were considered. In the first case, Casson fluid is treated as fluid with constant plastic dynamic viscosity (i.e. $\xi = 0$) and stratification parameter set to hypolimnion ($S_t = 0.8$). It is observed that the temperature distribution increases with an increase in the value of β throughout the fluid domain ($0 \leq \eta \leq 8$). In the second case, Casson fluid is treated as fluid with variable plastic dynamic viscosity (i.e. $\xi = 4$) without stratification (i.e. $S_t = 0$) this corresponds to epilimnion layer. The temperature decreases negligibly as β increases from non-Newtonian fluid to Newtonian fluid (i.e. $\beta \to \infty$). This result is in good agreement with a report on effects of Casson fluid parameter β, temperature dependent viscosity ξ and temperature dependent thermal-conductivity parameter ε over temperature profiles in [30]. Figure 12 illustrates the effects of thermal stratification parameter (S_t) on the temperature profiles of non-Newtonian Casson fluid ($\beta = 0.2$) when the heat is injected greatly by setting ($\xi = 5$), in the presence of internal heat generation on dimensionless space ($q1 = 4$) and intensity($n = 0.5$). It is found that the temperature decreases. This result can be traced to the fact that, as (S_t) increases, the wall temperature decreases, this effect dominate the temperature distribution. Figure 15 exhibits the temperature profiles for different values of intensity of exponentially decaying internal heat generation on dimensionless space. The temperature profiles decreases as n ranges from -0.08 to 0.10. Figure 18 exhibits the temperature profiles for different values of exponentially decaying internal heat generation parameter when $n = 0.5$. The temperature profiles increases as q1 ranges from -4 to 5. Figure 21 depicts the effect of magnetic parameter Ha with thermal stratification ($i.e.\ S_t = 0.8$) and without thermal stratification($i.e.\ S_t = 0$) on temperature gradient. In both cases, temperature distribution increases. Maximum temperature is observed very close to the wall when thermal stratification is at epilimnion (i.e. $S_t = 0$) and maximum temperature in a parabolic profiles is observed when adjusted to hypolimnion (i.e. $S_t = 0.8$).

4.3 Temperature gradient

The rate of heat transfer in a certain direction depends on the magnitude of the temperature gradient (the temperature difference per unit length or the rate of temperature changes) in that direction. The higher the temperature gradient is caused the higher the rate of heat transfers.

The effects of temperature dependent plastic dynamic viscosity parameter ξ on the temperature gradient as Casson fluid flows over a stretchable surface embedded in thermally stratified medium with suction is indicated in figure 4. With an increase in the value of parameter (ξ), the temperature gradient of Casson fluid decreases near the wall. Within $3.3 \leq \eta \leq 3.7$ turning point of each profile exist and temperature gradient increases thereafter.

From Figure 7 it is observed that as the temperature dependent variable thermal conductivity parameter (ε) increases, temperature gradient increases significantly within $0 \leq \eta \leq 2.9$. Within this interval, maximum value of the temperature gradient is obtained when $\varepsilon = 8$ (i.e. Casson fluid is treated as fluid with variable thermal conductivity) as -0.1435 at $\eta = 1.6$. When the flow is investigated again by using the high value of stratification parameter ($S_t = 0.8$), together with the same values of the remain parameters i.e. $\xi = 7$, $\beta = 0.2$, $G_r = 1$, $H_a = 0.2$, $0 \leq \varepsilon \leq 8$, $N = 0.1$, $P_r = 0.72$, $q_1 = 2$, $n = 0.5$ and $S = 0.3$; it is observed that ε has no significant effect on temperature gradient except within $0.68 \leq \eta \leq 3.6$ where the effect is slightly significant. When Casson fluid is treated as fluid with constant plastic dynamic viscosity (i.e. $\xi = 0$) and stratification parameter is set to hypolimnion ($S_t = 0.8$). It is observed that the temperature gradient increases close to the wall and decreases far away from the wall. In the second case, Casson fluid is treated as fluid with the variable plastic dynamic viscosity (i.e. $\xi = 4$) without stratification (i.e. $S_t = 0$) this corresponds to epilimnion layer. The corresponding effect on the temperature gradient $\theta'(\eta)$ and heat transfer coefficient $\theta'(\eta = 0)$ as β increases from non-Newtonian fluid to Newtonian fluid (i.e. $\beta \to \infty$) is presented in Figure 10. The temperature gradient increases significantly with an increase in stratification (Fig. 13). The corresponding effect of intensity of exponentially decaying internal heat generation on temperature gradient $\theta'(\eta)$ and heat transfer coefficient $\theta'(\eta = 0)$ as n increases is shown in Figure 16. The temperature gradient increases significantly with an increase in exponentially decaying internal heat generation parameter as q_1 ranges from -4 to 5. (see Fig. 19). Turning point is observed within $2.2 \leq \eta \leq 2.5$, thereafter, the temperature gradient decreases. The effect of Magnetic field parameter with and without thermal stratification on temperature gradient is shown in figure 22.

5. Conclusion

Laminar free convective MHD boundary layer flow of non-Newtonian Casson fluid flow over an exponentially stretching surface embedded in a thermally stratified medium has been studied. The numerical approach was utilized to study the effect of all the controlling parameters on the flow's velocity and temperature profiles in the boundary layer. The results show that:

i. An increase in the variable plastic dynamic viscosity parameter of Casson fluid would increase the velocity profiles, but it would decrease the magnitude of temperature throughout the domain and temperature gradient close to the wall in the boundary layer.

ii. An increase in the variable thermal conductivity parameter of Casson fluid would increase the velocity and temperature profiles; temperature gradient also increases near the wall.

iii. Based on the results of the present study, it can be concluded that the effect of Casson fluid parameter when treated as fluid which possess constant plastic dynamic viscosity; the velocity decreases, temperature distribution increases and temperature gradient increases (near the wall). And, when treated as temperature dependent variable plastic dynamic viscosity; the velocity profile increases, temperature distribution decreases and temperature gradient decrease (near the wall).

iv. Increasing the stratification parameter results in reduction of velocity and temperature profiles.

v. It can be concluded that the effect of intensity parameter embedded in the exponentially decaying heat source decreases both velocity and temperature profiles.

vi. Variation of exponentially decaying heat source parameter show significant effect on the thickness of the boundary layer profiles (i. e. velocity, temperature and temperature gradient).

vii. The magnetic field reduces the heat transfer rate, though it causes the increment in the temperature inside the boundary layer when the stratification parameter is adjusted to epilimnion and hypolimnion.

Acknowledgements

The author expresses his profound gratitude to the anonymous Reviewer for their valuable comments and suggestions.

Nomenclature

x Distance along the surface
y Distance perpendicular to the surface
u Velocity along $x-$ direction (Streamwise velocity)
v Velocity along $y-$direction (Wall normal velocity)
$B(x)$ Variable magnetic field
g Acceleration due to gravity
T_∞ Ambient temperature
T_o Reference temperature
T Fluid temperature
C_p Heat capacity at constant pressure
q_r Radiative heat flux in $y-$ direction
Q_o Coefficient of space dependent heat generation
L Reference length
U_o Reference velocity
P_y Fluid yield stress
$T_w(x)$ Prescribed surface temperature
$T_\infty(x)$ Variable free stream temperature
C_f Local skin friction
Nu Local Nusselt number
q_w Heat flux
G_{rm} Local modified Grashof related parameter
Ha Magnetic field parameter
Pr Prandtl number
N Thermal radiation parameter
$q1$ Space dependent internal heat source parameter
St Stratification parameter
n Intensity of exponentially decaying heat source

Greek Symbols

ξ Variable Plastic dynamic viscosity parameter
ε Variable thermal conductivity parameter
β Non-Newtonian Casson parameter

ϑ Kinematic viscosity
ρ Density
$\theta(\eta)$ Non-dimensional temperature
τ_w Shear stress
σ Electrical conductivity of Casson fluid
μ_b Plastic dynamic viscosity
${\mu_b}^*$ Plastic dynamic viscosity of the ambient fluid
κ Thermal conductivity
κ^* Thermal conductivity of the ambient fluid
σ^* Electric conductivity
β^+ Volumetric coefficient of thermal expansion
ψ Stream function
π Product of the deformation component
γ Constant related to temperature dependent μ_b
δ Constant related to temperature dependent κ
η Similarity variable
μ Dynamic Viscosity

Subscripts

o Reference temperature close to the surface
w Property at the wall
∞ Property at ambient

Reference

[1] Crane, L.J., Flow Past a Stretching Plate, Z. Angew Math. Phys., 21 (1970) 645-647.

[2] Mukhopadhyay, S., Boundary layer flow and heat transfer of a Casson fluid past a symmetric porous wedge with surface heat flux, Chin. Phys. B, 23 (2014) 1-5.

[3] Casson, N., Rheology of disperse systems in flow equation for pigment Oil-suspensions of the printing ink type, Rheology of disperse systems. C. C. Mill, Ed.. Pergamon Press, UK,(1959) 84-102.

[4] Bird, R. B., Dai,G.C., Yarusso, B. G., The rheology and flow of Viscoplastic materials, Rev. Chem. Eng., 1(1983) 1-70.

[5] Venkatesan, J., Sankar, D. S., Hemalatha, K., Yatim, Y., Mathematical Analysis of Casson Fluid Model for Blood Rheology in Stenosed Narrow Arteries, Journal of Applied Mathematics, (2013) 583-809.

[6] Tasaka, Y., Kudoh, Y., Takeda, Y., Yanagisawa, T., Experimental investigation of natural convection induced by internal heat generation, Journal of Physics IOP: Conference Series, 14 (2005) 168–179.

[7] Crepeau, J. C., Clarksean, R., Similarity solutions of natural convection with internal heat generation, Transactions of ASME – Journal of Heat Transfer, 119(1997) 184-185.

[8] Salem, A. M., El-Aziz, M. A., MHD-mixed convection and mass transfer from a vertical stretching sheet with diffusion of chemically reactive species and space- or temperature-dependent heat source, Canadian Journal of Physics, 85 (2007) 359–373.

[9] Salem, A. M., El-Aziz, M. A., Effect of Hall currents and chemical reaction on hydromagnetic flow of a stretching vertical surface with internal heat generation/absorption, Applied Mathematical Modelling, 32 (2008) 1236–1254.

[10] Moorthy, M. B. K., Senthilvadivu, K., Effect of variable viscosity on free flow of non-Newtonian power-law fluids along a vertical surface with thermal stratification, archives of thermodynamics, 33 (2012) 109–121.

[11] Murthy, P. V. S. N., RamReddy, Ch., Chamkha, A. J., Rashad, A. M., Magnetic effect on thermally stratified nanofluid saturated non-Darcy porous medium under convective boundary condition, International Communications in Heat and Mass transfer, 47 (2013) 41 - 48.

[12] Mukhopadhyay, S., MHD boundary layer flow and heat transfer over an exponentially stretching sheet embedded in a thermally stratified medium, Alexandria Engineering Journal, 52 (2013) 259–265.

[13] RamReddy, Ch., Murthy, P.V.S.N., Rashad, A. M., Chamkha, A. J., Numerical study of thermally stratified nanofluid flow in a saturated non-Darcy porous medium, The European Physical Journal Plus 129, 25 (2014).

[14] Mukhopadhyay, S., Casson fluid flow and heat transfer over a nonlinearly stretching surface, Chin. Phys. B., 22 (2013) 1-5.

[15] Hayat, T., Shehzadi, S. A., Alsaedi, A., Soret and Dufour effects on magnetohydrodynamic (MHD) flow of Casson fluid, Appl. Math. Mech. Engl. Ed., 33 (2012) 1301-1312.

[16] Chamkha, A. J., Mujtaba, M., Quadri, A., Issa, C., Thermal radiation effects on MHD forced convection flow adjacent to a non-isothermal wedge in the presence of a heat source or sink, Heat and Mass Transfer of Springer-Verlag, 39 (2003) 305–312.

[17] Anyakoha, M. W., New School Physics, 3rd Edition, Africana First Publisher Plc. (2010).

[18] Batchelor, G. K., An Introduction to Fluid Dynamics, Cambridge University Press, London, (1987).

[19] Vajravelu, K., Prasad, K. V., Chiu-On, N., The effect of variable viscosity on the flow and heat transfer of a viscous Ag-water and Cu-water Nanofluids, Journal of Hydrodynamics, 25 (2012) 1-9.

[20] Salem A. M., Fathy, R., Effects of variable properties on MHD heat and mass transfer flow near a stagnation point towards a stretching sheet in a porous medium with thermal radiation, Chin. Phys. B, 21 (2012) 1- 11.

[21] Layek, G. C., Mukhopadhyay, S., Samad, Sk. A., Study of MHD boundary layer flow over a heated stretching sheet with variable viscosity, International

Journal of Heat and Mass Transfer, 48 (2005) 4460 - 4466.

[22] Gill, S., A Process for the Step-by-Step Integration of Differential Equations in an Automatic Digital Computing Machine, Proceedings of the Cambridge Philosophical Society, 47 (1951) 96 - 108.

[23] Finlayson, B. A., Nonlinear Analysis in Chemical Engineering, McGraw-Hill, New York (1980).

[24] Na, T.Y., Computational Methods in Engineering Boundary Value Problems, Academic Press, New York, (1979).

[25] Hoffman, J. D., Numerical Methods for Engineers and Scientists, McGraw-Hill, New York. (1992).

[26] Animasaun, I. L., Dynamics of Unsteady MHD Convective Flow with Thermophoresis of Particles and Variable Thermo-Physical Properties past a Vertical Surface Moving through Binary Mixture, Open Journal of Fluid Dynamics, 5 (2015) 106-120.

[27] Bidin, B., Nazar, R., Numerical solution of the boundary layer flow over an exponentially stretching sheet with thermal radiation, European Journal of Scientific Research, 33(2009) 710–717.

[28] Nadeem, S., Zaheer, S., Fang, T., Effects of thermal radiation on the boundary layer flow of a Jeffrey fluid over an exponentially stretching surface, Numerical Algorithms, (2011) 187-205.

[29] Pramanik, S., Casson fluid flow and heat transfer past an exponentially porous stretching surface in presence of thermal radiation, Ain Shams Engineering Journal, 5 (2014) 205-212.

[30] Animasaun, I.L., Effects of thermophoresis, variable viscosity and thermal conductivity on free convective heat and mass transfer of non-darcian MHD dissipative Casson fluid flow with suction and nth order of chemical reaction, Journal of the Nigerian Mathematical Society, 34 (2015) 11–31.